ACCSCIENCE PUBLISHING

International Journal of Bioprinting

RESEARCH ARTICLE

Laponite-reinforced conductive GelMA–-Ionic liquid nanocomposite hydrogels for high-fidelity extrusion printing and localized neurotrophic delivery

Jiarui Zhou[1,2], Kamil Elkhoury[1], Abhay Menon[1], and Sanjairaj Vijayavenkataraman[1,2]*

[1]The Vijay Lab, Division of Engineering, New York University Abu Dhabi, Abu Dhabi, United Arab Emirates

[2]Department of Mechanical and Aerospace Engineering, Tandon School of Engineering, New York University, Brooklyn, New York, United States of America

Abstract

The development of advanced hydrogel systems capable of precise three-dimensional (3D) printing and controlled therapeutic delivery is critical for next-generation biofabrication strategies. In this study, we present a laponite-reinforced gelatin methacryloyl (GelMA)/ionic liquid hydrogel engineered to simultaneously improve printability and sustained release of bioactive molecules. The incorporation of laponite nanoparticles markedly enhances rheological characteristics, including viscosity, shear-thinning behavior, and structural fidelity, facilitating high-resolution extrusion-based 3D printing. Specifically, the laponite concentration was limited to 1% *w/v* to preserve the soft mechanical environment (<3 kPa) essential for neural tissue while sufficiently improving rheological properties for processing. Beyond its mechanical and processing advantages, the hydrogel enables the prolonged release of retinoic acid and glial cell line-derived neurotrophic factor, promoting the proliferation and neuronal differentiation of N2A cells. This dual-functional platform demonstrates significant potential for the fabrication of complex, cell-instructive scaffolds, offering a versatile approach for applications where structural precision and localized drug delivery are essential.

Keywords: Gelatin methacryloyl; Conductive hydrogel; Ionic liquid; Neural tissue; Three-dimensional printing; Extrusion

***Corresponding author:**
Sanjairaj Vijayavenkataraman (vs89@nyu.edu)

Citation: Zhou J, Elkhoury K, Menon A, Vijayavenkataraman S. Laponite-reinforced conductive GelMA–-Ionic liquid nanocomposite hydrogels for high-fidelity extrusion printing and localized neurotrophic delivery. *Int J Bioprint.* 2026:12(2):026020009. doi: 10.36922/IJB026020009

Received: January 7, 2026

Revised: January 7, 2026

Accepted: February 12, 2026

Published online: April 17, 2026

1. Introduction

Three-dimensional (3D) printing has become a powerful tool in tissue engineering, regenerative medicine, and disease modeling, enabling the fabrication of complex, customizable structures.[1–3] Among the various techniques, extrusion-based 3D printing is especially attractive due to its scalability, low cost, and suitability for *in situ* applications.[4–6] Hydrogels are frequently employed as bioinks for this purpose, owing to their biocompatibility, excellent water retention, and structural similarity to the extracellular matrix (ECM).[7] However, printing soft hydrogels requires fine-tuning of

their mechanical, rheological, and biological properties to fall within the "biofabrication window," critical for achieving high-fidelity constructs without compromising cell viability.[7–9]

Gelatin methacryloyl (GelMA), a photocrosslinkable hydrogel, is widely used due to its biocompatibility and tunable stiffness.[10,11] While high-concentration GelMA (>10%) can be printed with reasonable fidelity, softer matrices (<10 kPa) based on low GelMA content remain difficult to extrude consistently due to insufficient viscosity.[12] This limitation restricts the fabrication of soft, cell-instructive microenvironments, which are especially relevant for neural applications.

To address this, nanoparticles such as laponite have been incorporated into hydrogel formulations to enhance rheology without compromising biocompatibility.[13–15] Laponite is a synthetic silicate nanoplatelet (~25 nm diameter, 1 nm thickness) with charge heterogeneity that enables self-assembly into shear-thinning, thixotropic gels.[16–20] Its anisotropic surface charges also enable interaction with diverse biomolecules, making it effective for sustained release of drugs and growth factors.[21–23] These properties make laponite a versatile additive for improving both printability and biofunctionality of hydrogel systems. However, it is important to note that the biocompatibility of laponite is concentration-dependent. While low concentrations support cell survival, elevated levels can compromise the viability of encapsulated cells.[24]

Nerve tissue engineering requires scaffolds that not only mimic the ECM but also support electrical signal conduction, a key aspect of neuronal function and regeneration.[25] Current clinical treatments, including autografts, allografts, and direct coaptation, face challenges, such as donor site morbidity, immune rejection, and limited availability.[26–29] Nerve guidance conduits offer a promising alternative, particularly when engineered to combine structural integrity, bioactivity, and electroconductivity.[30,31] Conductive biomaterials can promote neurite outgrowth, synaptic activity, and overall functional recovery.[32] In this context, ionic liquids (ILs) have emerged as promising candidates due to their intrinsic ionic conductivity and tunable chemical structure.[33,34]

Ionic liquids are a class of liquid salts composed of ions with a melting point below 100 °C.[35] ILs have gained significant attention as conductive additives in biomaterials, offering distinct advantages such as high ionic conductivity, thermal stability, negligible vapor pressure, and versatile solubility.[33,36] To enhance clinical relevance, recent efforts have focused on bio-ILs designed for superior biocompatibility. Among these, choline-based formulations are especially promising; as a critical nutrient and integral cell membrane component, choline confers low toxicity and high biocompatibility.[37] Consequently, prior studies have successfully incorporated choline-based ILs into hydrogel matrices, such as GelMA and polyethylene glycol diacrylate, to engineer bioactive composite systems.[38,39]

Previously, we developed a multi-layered nerve guidance conduit combining a polycaprolactone shell with a GelMA hydrogel core to provide mechanical support and a biomimetic microenvironment.[40] However, the system lacked sufficient conductivity, limiting its applicability in electrically responsive tissues.

In this study, we present a GelMA-based hydrogel system enhanced with ILs and laponite to address critical challenges in extrusion-based bioprinting, including print fidelity, sustained drug release, and electrical functionality. Laponite improves rheological performance, printability, and drug release, while ILs contribute to conductivity and biocompatibility. The hydrogel's cytocompatibility was validated through N2A cell culture studies. Together, these advances establish the GelMA/IL/laponite hydrogel as a promising platform for 3D-printed electroconductive scaffolds for neural repair and regeneration.

2. Materials and methods

2.1. Materials

Gelatin from porcine skin (Type A, 300 bloom), methacrylic anhydride (MA), collagenase type II (C2-22-1G), 4',6-diamidino-2-phenylindole (D9542; 5 mg), penicillin–streptomycin solution (P4333, 100 mL), lithium phenyl (2,4,6-trimethylbenzoyl) phosphinate (LAP; 5 g), and laponite nanoclay (500 g) were obtained from Sigma Aldrich (United States of America [USA]). AlamarBlue™ HS Cell Viability Reagent and LIVE/DEAD™ Viability/Cytotoxicity Kit for mammalian cells were purchased from Invitrogen (USA). Dulbecco's Modified Eagle Medium (DMEM), Dulbecco's phosphate-buffered saline (DPBS), fetal bovine serum (FBS), and trypsin–ethylenediaminetetraacetic acid were obtained from Gibco (USA). All-trans-retinoic acid (97%; 5 g) was purchased from Thermo Scientific (USA). Human glial cell line-derived neurotrophic factor (GDNF) enzyme-linked immunosorbent assay kit was purchased from Abcam (United Kingdom). N2A cells were kindly supplied by Prof. Dan Ohtan Wang (NYU Abu Dhabi, United Arab Emirates).

2.2. Gelatin methacryloyl synthesis

Gelatin methacryloyl was synthesized following a previously reported protocol.[41] In brief, 10% *w*/*v* of gelatin was dissolved in DPBS at 50 °C. MA was then added

gradually (0.125 mL/g), while maintaining constant stirring at 50 °C for two hours. To halt the reaction, twice the volume of pre-warmed DPBS (40 °C) was added. The resulting mixture was placed in dialysis tubing with a molecular weight cutoff of 12–14 kDa and dialyzed at 50 °C against deionized water to eliminate excess MA. The water was changed twice a day for seven days. The solution was passed through a 0.2 μm filter, freeze-dried, and stored at 4 °C until further use.

2.3. Gelatin methacryloyl/ionic liquid/laponite synthesis and hydrogel fabrication

To prepare the hydrogel solution, GelMA (5% *w*/*v*), choline–bicarbonate (IL, 20% *v*/*v*), and LAP (0.25% *w*/*v*) were dissolved at a temperature of 37 °C in DPBS. This solution was then mixed with laponite powder at varying concentrations of 0.5% and 1% *w*/*v*. To prepare the hydrogels, the hydrogel precursor solution was subsequently cross-linked using ultraviolet light (Form Cure, light-emitting diode [LED] power: 39 W; Formlabs Inc., USA) for two minutes at 405 nm.

2.4. Rheological analysis

Dynamic mechanical analysis (MCR 702e MultiDrive, Anton Paar Inc., Austria) was used to perform the rheology test of 5% *w*/*v* GelMA/20% *v*/*v* IL solution with different concentrations of laponite (before cross-linking). Parallel plates with 25 mm and 50 mm diameters were used. All tests were performed at room temperature, around 22 °C. The linear viscoelasticity range (LVER) was first established through an amplitude sweep spanning from 0.1% to 1,000%. Subsequently, 3-interval thixotropy tests (3TT) were performed at a high shear rate of 100 Hz and a low shear rate of 0.1 Hz within each sample's LVER range. Photorheology was performed using an LED light (405 nm) source placed at a set distance of 3 cm from the rheometer plate for two minutes. Finally, the maximum linear viscosity value was identified, and a frequency sweep ranging from 0.1 Hz to 100 Hz was conducted, employing a strain level below the LVER range, to determine the shear storage modulus, shear loss modulus, and complex viscosity. The shear thinning properties were further evaluated using a power law (Equation (1)) to define the flow behavior index and the flow consistency index:

$$\sigma = K\dot{\gamma}^{n} \tag{1}$$

where K (mPa·s) is the flow consistency index, and n is the flow behavior index.

2.5. Scanning electron microscopy

The GelMA/IL/laponite samples were frozen overnight at −80 °C, followed by lyophilization for 72 h. The dried samples were then sectioned to expose the cross-sectional area and were imaged at 5 kV. The mean sizes of the GelMA/IL/laponite hydrogel pores were analyzed from a group of three samples (n = 50 across three samples). The scanning electron microscopy (SEM; FEI Quanta 3D FEG Dual Beam Electron Microscope Hillsboro, USA) images of the hydrogel samples were obtained at 10 kV. Sputter gold coating was performed before image capture to increase the electron density of all samples.

2.6. Conductivity test of gelatin methacryloyl/ionic liquid/laponite pre-solution and hydrogel

Electrical conductivity tests were conducted on GelMA/IL/laponite hydrogels with varying concentrations of laponite. A volume of 0.8 mL of the GelMA/IL/laponite hydrogel solution was dispensed into a rectangular mold, which had been fabricated using a Form 3 3D printer (FormLabs Inc., USA). Conductivity measurements were carried out using a four-probe electrical station. Probes were strategically placed within the hydrogel precursor at consistent inter-probe distances. Subsequently, *in situ* cross-linking was performed using an LED light for two minutes at a wavelength of 405 nm. A current ranging from 0.01 mA to 0.2 mA was applied using the outer two probes, while the voltage response was recorded by the inner two probes. The conductivity of the hydrogel precursor was determined using Equation (2):

$$\sigma = \frac{L}{RA} \tag{2}$$

where L is the probe-to-probe distance, R is the resistance, and A is the conductor cross-sectional area.

2.7. Mechanical characterization of the gelatin methacryloyl/ionic liquid/laponite hydrogel

Mach-1 v500cs (Biomomentum Inc., Canada) was used to perform the compression test with a 17 N load cell. The GelMA/IL/laponite hydrogel cylinder with a flat surface finish was fabricated and cross-linked using ultraviolet light. The hydrogel thickness was assessed using the Mach-1 machine. All samples were subjected to a total compressive strain of 70% at a rate of 10% strain per second. For modulus evaluation, data within the 10–20% strain range were analyzed. Throughout the testing process, hydrogels were maintained in a hydrated condition.

2.8. Collagenase degradation

Degradation tests on GelMA/IL/laponite hydrogels with laponite concentrations of 0%, 0.5%, and 1% were conducted at intervals of 0, 6, 12, 24, and 48 h. The hydrogels were cross-linked for two minutes at 405 nm (Form Cure, LED power: 39 W; Formlabs Inc., USA) and subsequently kept at 37 °C overnight in PBS before undergoing the degradation tests.

Subsequently, the PBS was replaced with the collagenase solution (5 U/mL solution that corresponds to 125 U/mg), and the hydrogels were collected, lyophilized, and weighed at each specified time point. The average mass at each time point was normalized to the initial (0-h) value and plotted to illustrate changes over time.

2.9. Extrusion-based three-dimensional printing of hydrogel

Grids measuring 10 mm × 10 mm and 15 mm × 15 mm, circles with diameters of 5 mm, 10 mm, and 20 mm, and the letters "NYU" were designed and printed using a RegenHu Discovery bioprinter (Swiss) with an extrusion-based printhead. A hydrogel composed of 5% GelMA and 20% IL was used as a control to compare the printability with a hydrogel consisting of 5% GelMA, 20% IL, and 1% laponite. The nozzle diameter was 0.61 mm, and the optimized pressures were 0.01 MPa for the control and 0.02 MPa for the GelMA/IL/laponite hydrogel. The printed structures were immediately cross-linked under 405 nm for two minutes. All procedures were performed at room temperature. The printing of a 2 cm equilateral triangle and 10 mm thickness was achieved by photocrosslinking each layer for one minute.

2.10. Printability analysis of various structures

The images of the printed structures were captured under bright light. Line width was measured using ImageJ (version 1.54h) (n = 10 per structure). Relative line length was normalized to the nozzle diameter (0.61 mm).

2.11. Drug release of glial cell line-derived neurotrophic factor and retinoic acid

To evaluate the release kinetics of retinoic acid from GelMA/IL/laponite hydrogels, 18 μg of retinoic acid was mixed with GelMA/IL hydrogel and GelMA/IL/laponite hydrogel at laponite concentrations of 0.5% and 1%. For the retinoic acid release test, 300 μL of the hydrogel pre-solution was injected into a 1.5 mL Eppendorf tube and cross-linked as previously described. One mL of PBS solution was added to the tube, which was then incubated at 37 °C. At specified time points (1, 3, 6, 12, 24, 48, and 96 h), the supernatant was collected and replaced with fresh normal saline. The concentration of released retinoic acid in the supernatant was measured using a microplate reader (BioTek Instruments, Inc., USA) at 432 nm. The net drug release at each time point was calculated by multiplying the drug concentration by the supernatant volume. The accumulated drug release was calculated by summing the net drug release at each time point.

A similar method was applied for the GDNF release analysis. At specified time points (3, 6, 12, 24, 48, 96, and 168 h), the supernatant was collected and replaced with fresh normal saline. The concentration of GDNF was measured using an enzyme-linked immunosorbent assay kit according to the manufacturer's instructions. The net drug release and accumulated drug release were calculated based on the method mentioned above.

2.12. Two-dimensional cell culture of N2A cells

N2A cells were cultured in T25 flasks, each initially seeded with 250,000 cells. The cell culture medium, comprising DMEM supplemented with 10% FBS and 1% penicillin–streptomycin, was prepared and refreshed bi-daily. The cells were maintained at 37 °C in a 5% carbon dioxide incubator and were harvested on Day 3 for subsequent two-dimensional (2D) N2A cells seeding on GelMA/IL/laponite hydrogels.

2.13. N2A cells seeding onto gelatin methacryloyl/ionic liquid/laponite hydrogel

A volume of 0.3 mL of the GelMA/IL/laponite hydrogel solution was pipetted into each well of a 24-well plate and subsequently cross-linked for two minutes at 405 nm. Following cross-linking, 1 mL of pre-warmed PBS was added to each well, and the plate was incubated overnight at 37 °C to allow the hydrogel to swell. Prior to cell seeding, the PBS was removed, and 10,000 cells were seeded per well. Each well then received 1 mL of cell culture medium, which was refreshed bi-daily. The 24-well plate was maintained in a 5% carbon dioxide incubator at 37 °C.

2.14. Cell viability of N2A cells seeded in hydrogels

Cell viability of N2A cells cultured on GelMA/IL/laponite hydrogels was evaluated on Day 1 and Day 3 using the LIVE/DEAD cell viability assay. The staining solution was prepared by mixing 1 μL of calcein acetoxymethyl ester and 4 μL of ethidium homodimer-1 with 2 mL of PBS. Prior to staining, the hydrogel was rinsed with pre-warmed PBS. Subsequently, the staining solution was applied to the scaffolds within the well plate and incubated for 30 min at 37 °C. After incubation, the hydrogels were transferred from the well plate onto a glass slide and imaged using a ZOE Fluorescent Cell Imager (Bio-Rad Laboratories Inc., USA). ImageJ software was used to analyze the images to assess cell viability, employing Equation (3):

$$Cell\ viability = \frac{Live\ cells}{Live\ cells + dead\ cells} \times 100 \quad (3)$$

2.15. Two-dimensional cell differentiation of N2A cells into neurons

N2A cells were cultured using cell culture medium in T25 flasks as described in Section 2.14 on Day 1. At the end of Day 1, the medium was replaced with a cell differentiation

medium, consisting of DMEM supplemented with 0.1% FBS, 20 μM retinoic acid, and 1% penicillin–streptomycin. The cell differentiation medium was changed every two days. The cells were maintained at 37 °C in a 5% carbon dioxide incubator and were harvested on Day 3 after induction for the 2D neurons seeding on GelMA/IL/laponite hydrogels.

2.16. Neurite length measurement and relative cell quantity measurements

N2A cells were initially cultured in 6-well plates and differentiated as previously described. Brightfield images were captured on Day 1 before differentiation and on Day 3 after differentiation, using the ZOE Fluorescent Cell Imager (Bio-Rad Laboratories Inc., USA). Neurite length was measured using ImageJ (n = 10 per sample). Relative cell quantity was also measured using ImageJ and normalized to the cell quantity on Day 1 before differentiation.

2.17. Seeding of differentiated neurons onto gelatin methacryloyl/ionic liquid/laponite hydrogel

Differentiated neurons were seeded onto the GelMA/IL/laponite hydrogel as described in Section 2.13. Subsequently, 1 mL of cell differentiation medium was added to each well in place of the cell culture medium, which was refreshed bi-daily. The 24-well plate was maintained in a 5% carbon dioxide incubator at 37 °C. A volume of 0.3 mL of the GelMA/IL/laponite hydrogel solution was pipetted into each well of a 24-well plate and subsequently cross-linked for two minutes at 405 nm. Following cross-linking, 1 mL of pre-warmed PBS was added to each well, and the plate was incubated overnight at 37 °C to allow the hydrogel to swell. Prior to cell seeding, the PBS was removed, and 10,000 cells were seeded per well. Each well then received 1 mL of cell differentiation medium, which was refreshed bi-daily. The 24-well plate was maintained in a 5% carbon dioxide incubator at 37 °C.

2.18. Cell proliferation in the cell-seeded hydrogel

Cell viability and proliferation of N2A cells and differentiated neurons on GelMA/IL/laponite hydrogels were assessed using the Alamar Blue assay, with measurements taken on Day 1 and Day 3. Initially, the culture medium was removed from each well containing the GelMA/IL/laponite hydrogel, and a pre-warmed mixture of fresh medium and Alamar Blue reagent, in a 10:1 ratio, was added. The hydrogels were then incubated in darkness for four hours. Subsequently, 100 μL aliquots were extracted three times from this mixture and stored at −80 °C until analysis at all designated time points. Absorbance readings were obtained using a microplate reader (BioTek Instruments, Inc., USA) at a primary wavelength of 570 nm and a reference wavelength of 600 nm. The percentage reduction of Alamar Blue, indicative of cell culture proliferation, was calculated using colorimetric equations provided by BioRad (USA).

2.19. Statistical analysis

All results are presented as mean ± standard deviation. Statistical significance was assessed using one-way or two-way analysis of variance, as appropriate. Differences were considered significant based on the following criteria: $p < 0.05$ (*), $p < 0.01$ (**), and $p < 0.001$ (***). Results that were not statistically significant are denoted as ns.

3. Results

3.1. Rheological characterizations of gelatin methacryloyl/ionic liquid/laponite solution

Hydrogel formulations consisting of 5% GelMA/20% IL with laponite concentrations of 0%, 0.5%, and 1% (Figure 1A) were thoroughly mixed and assessed for their rheological properties.

Figure 1B displays the frequency sweep results for the hydrogels, covering a range from 100 Hz to 0.1 Hz. All groups exhibited shear-thinning behavior, as indicated by the decrease in complex viscosity with increasing shear rate. Each group displayed a flow behavior index below 1, characteristic of non-Newtonian fluids (Figure 1C). Notably, the flow behavior index decreased from 0.38 to 0.30 as the laponite concentration increased from 0% to 1%. A flow behavior index below 0.33 is considered ideal for materials used in extrusion-based 3D printing. Furthermore, the flow consistency index for the 5% GelMA/20% IL/1% laponite hydrogel was 10 times higher than that of the 5% GelMA/20% IL control, indicating a significantly higher initial viscosity at low shear rates (Figure 1D).

The 3TT was conducted to emulate the extrusion process and evaluate the ink's shape recovery post-extrusion at both low (0.1 Hz) and high (100 Hz) shear rate cycles (Figure 1E). With the addition of laponite, the hydrogel demonstrated faster recovery from high to low shear rates. This stability and rapid recovery, along with the increased flow consistency index, indicate that the addition of laponite significantly enhanced the ability of the hydrogel to maintain shape fidelity after printing.

To evaluate the cross-linking kinetics of GelMA/IL-based hydrogels with and without laponite, oscillatory rheological tests were conducted under LED light at 405 nm (Figure 1F). The hydrogel solutions were allowed to stabilize for three minutes on the parallel plate before being cross-linked for two minutes, followed by an

additional five minutes of stabilization. Across all groups, the storage modulus increased upon light activation. Although increasing the concentration of laponite raised the hydrogel's viscosity both before and after cross-linking, the photocrosslinkable nature of the hydrogel remained unaffected.

3.2. Morphological and mechanical characterization of gelatin methacryloyl/ionic liquid/laponite hydrogel

The SEM images of freeze-dried GelMA/IL hydrogels with varying laponite concentrations are presented in Figure 2A, illustrating their inherently porous structure. The

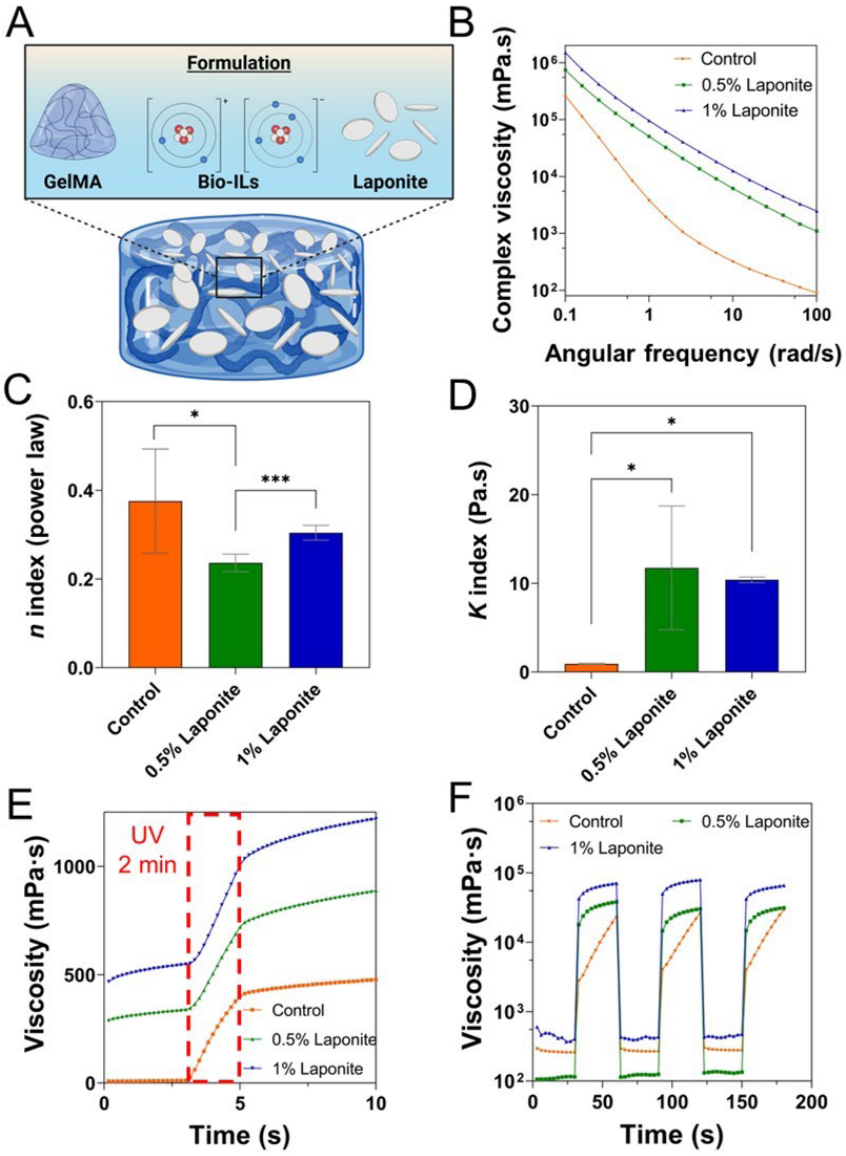

Figure 1. Rheological characterization of hydrogels. (A) Schematic representation of the GelMA/IL/laponite formulation. Created in BioRender. Elkhoury, K. (2026) https://BioRender.com/2u9y1d1. (B) Complex viscosity of 5% GelMA/20% IL/0–1% laponite solution at a shear rate from 0.1 Hz to 100 Hz. Shear-thinning behavior calculated using the power law model. (C) *n* index and (D) *K* index for 5% GelMA/20% IL/0–1% laponite solution. (E) Three-interval thixotropy test from low shear (0.1 Hz) to high shear rate (100 Hz) cycles of 30-s intervals for 5% GelMA/20% IL/0–1% laponite solutions. (F) Oscillatory-time sweeps of 5% GelMA/20% IL/0–1% laponite measuring storage modulus G' during cross-linking of precursor solutions using visible light under 405 nm for two minutes. All data are expressed as mean ± standard deviation. Significance is indicated as * ($p < 0.05$), *** ($p < 0.001$), and ns (not significant).

Abbreviations: GelMA: Gelatin methacryloyl; IL: Ionic liquid; UV: Ultraviolet.

incorporation of laponite did not cause significant variance in the average pore size (Figure 2B).

Mechanical compression tests were conducted to determine the Young's modulus from the elastic region of the stress–strain curves depicted in Figure 2C,D. The Young's modulus progressively increased from 2.21 ± 0.07 kPa to 2.56 ± 0.18 kPa as the laponite concentration increased from 0% to 1%. All test groups recorded a Young's modulus below 10 kPa, which is considered ideal for applications in soft tissue engineering.[42–44]

3.3. Biodegradability, conductivity, and drug release ability of gelatin methacryloyl/ionic liquid/laponite hydrogel

Figure 3A illustrates the enzymatic degradation rates among all test groups. The degradation trends for the GelMA/IL control and the GelMA/IL/0.5% laponite were similar. However, the 5% GelMA/20% IL/1% laponite group exhibited a significant decrease in mass loss percentage compared to the other groups. Specifically, at the final time point, the mass loss for the 5% GelMA/20% IL/1% laponite group was reduced by 39% compared to the 5% GelMA/20% IL control, indicating enhanced stability against enzymatic degradation with higher laponite concentration.

The conductivity measurements of GelMA/IL, GelMA/IL/0.5% laponite, and GelMA/IL/1% laponite samples showed no significant differences among the groups (Figure 3B). All formulations exhibited a conductivity value around 30 mS/cm, indicating that the addition of laponite at concentrations of 0.5% and 1% did not noticeably affect the overall ionic conductivity of the gels.

The *in vitro* release profiles of GDNF and retinoic acid are shown in Figure 3C,D. For GDNF, there was minimal difference in cumulative release within the first 24 h, with an average of 9.7 pg released by that time. On Day 2, the 5% GelMA/20% IL control released an average of 13.3 pg, while the 5% GelMA/20% IL/1% laponite hydrogel released 12.5 pg. By Day 7, the cumulative drug release for the 5% GelMA/20% IL/1% laponite hydrogel was 17.5% lower than that of the 5% GelMA/20% IL control.

A similar trend was observed for the retinoic acid release experiment. At the last time point (Day 3), the cumulative drug release for the 5% GelMA/20% IL/1%

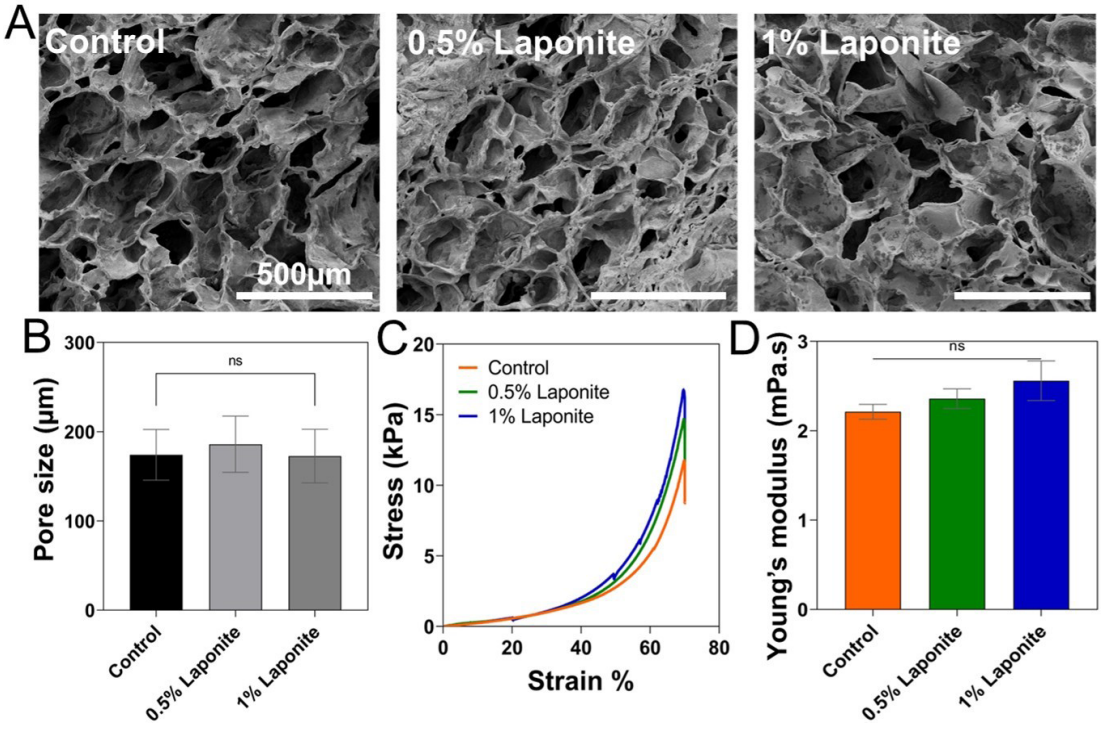

Figure 2. Morphological and mechanical characterization of hydrogels. (A) SEM images of 5% GelMA/20% IL/0–1% laponite hydrogel. Scale bar: 500 μm; magnification: 100×. (B) Average pore sizes of 5% GelMA/20% IL/0–1% laponite hydrogel. (C) Stress–strain curves for 5% GelMA/20% IL/0–1% laponite hydrogel. (D) Young's modulus of 5% GelMA/20% IL/0–1% laponite hydrogel. All data are expressed as mean ± standard deviation. Significance is indicated as *($p < 0.05$) and ns (not significant).
Abbreviations: GelMA: Gelatin methacryloyl; IL: Ionic liquid; SEM: Scanning electron microscopy.

laponite hydrogel was 6.32 μg, which was 19.4% lower than the 7.84 μg released by the 5% GelMA/20% IL control. Notably, the cumulative release profile of the 5% GelMA/20% IL/1% laponite hydrogel began to deviate from the 5% GelMA/20% IL control after six hours and continued to release more slowly until Day 3.

3.4. Printability of gelatin methacryloyl/ionic liquid/laponite hydrogel

The printed structures using both control (GelMA/IL) and GelMA/IL/laponite hydrogels under different designs are shown in Figure 4A,B. Structures printed with the GelMA/IL/laponite hydrogel maintained better structural integrity, displaying clear voids in the grid structure and distinct separation between the circles. In contrast, structures printed with the control hydrogel (GelMA/IL) were either partially or fully merged.

The normalized line width of the control hydrogel was more than twice that of the GelMA/IL/laponite hydrogel (Figure 4C). Furthermore, when comparing the normalized line width within the same design but with different dimensions, we observed that the normalized line width decreased as the structure dimension decreased (Figure 4D,E). The printing of a stable multi-layered triangular prism composed of 20 layers with a height of ~10 mm was achieved, as shown in Figure 4F,G, using the

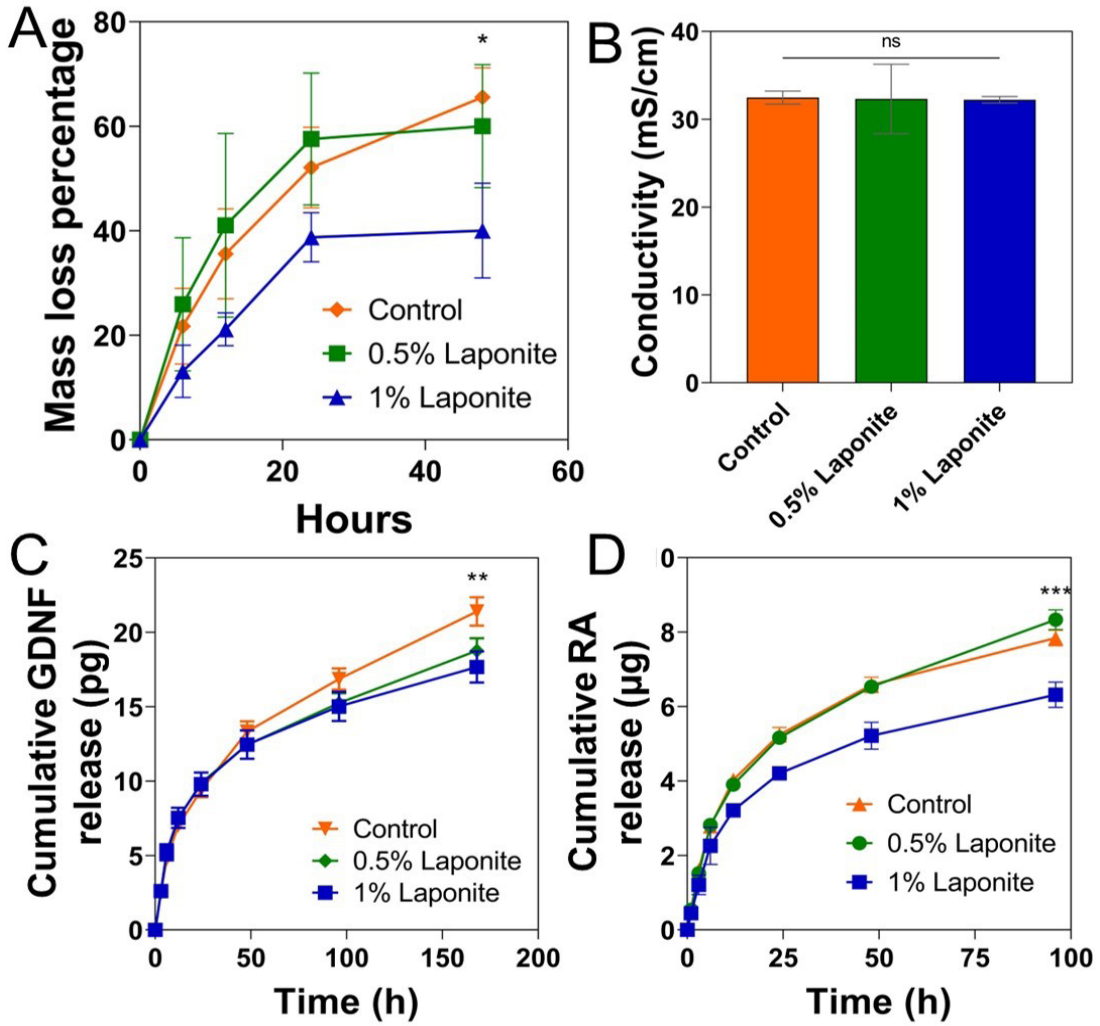

Figure 3. Degradative, conductive and drug release properties. (A) Enzymatic (5 U/mL collagenase) degradation rate of 5% GelMA/20% IL/0–1% laponite hydrogel. (B) Conductivity of 5% GelMA/20% IL/0–1% laponite hydrogel. The cumulative release of (C) GDNF and (D) retinoic acid (RA) from GelMA/IL/laponite hydrogels. All data are expressed as mean ± standard deviation. Significance is indicated as *($p < 0.05$), **($p < 0.01$), ***($p < 0.001$), and ns (not significant).
Abbreviations: GDNF: Glial cell line-derived neurotrophic factor; GelMA: Gelatin methacryloyl; IL: Ionic liquid.

strategy of photocrosslinking of each printed layer for one minute.

3.5. Cell viability and cell proliferation of two-dimensional N2A cells seeded in gelatin methacryloyl/ionic liquid/laponite hydrogel

Cell viability on the hydrogel was evaluated on Days 1 and 3. Figure 5A depicts the distribution of live cells on the hydrogel surface. N2A cells successfully adhered to the hydrogel on Day 1 across all groups, formed colonies, and continued to grow until Day 3. All groups maintained a high live cell viability ratio exceeding 90% by Day 3 (Figure 5B). Cell proliferation was assessed using the Alamar Blue assay, which showed a significant increase in cell proliferation from Day 1 to Day 3 across all groups (Figure 5C).

3.6. N2A differentiation to neurons and cell proliferation of two-dimensional seeded neurons on gelatin methacryloyl/ionic liquid/laponite hydrogel

The morphology of N2A cells on Day 3, both with and without differentiation, is shown in Figure 5D. The neurite outgrowth length of the differentiated neurons was six times greater than that of the undifferentiated N2A cells (Figure 5E). The relative cell density remained stable from Day 1 to Day 3 for the differentiated neurons. In contrast, the relative cell density of the undifferentiated N2A cells increased by 4.8 times on Day 3 compared to Day 1 (Figure 5F).

Cells activated to differentiate were harvested on Day

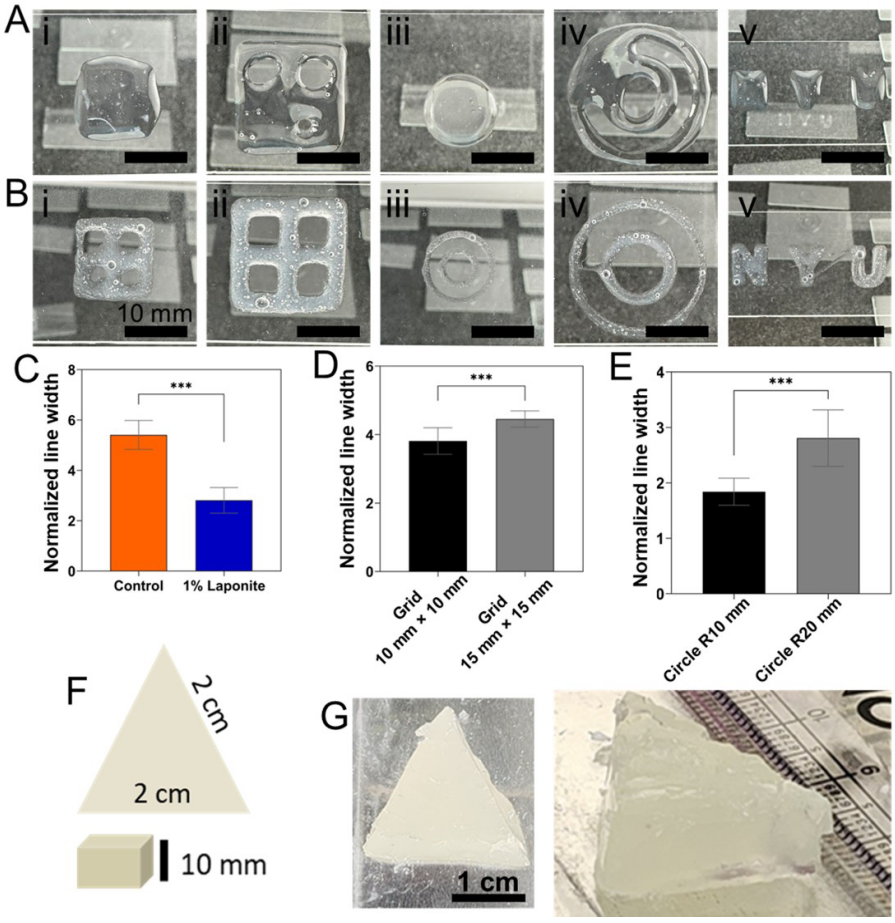

Figure 4. Extrusion printing of hydrogels. Three-dimensional-printed structures with (A) GelMA/IL hydrogel and (B) GelMA/IL/laponite hydrogel under various designs: (i) 10 mm × 10 mm grid; (ii) 15 mm × 15 mm grid; (iii) circle with diameters of 5 mm and 10 mm; (iv) circles with diameters of 10 mm and 20 mm; and (v) letters of "NYU." Scale bar: 10 mm. (C) The normalized line width of control and GelMA/IL/laponite hydrogel. The normalized line width within the same designs but different dimensions: (D) grid design and (E) circle design. (F) Computer-aided design model and (G) photographs of a 2 cm equilateral triangular printed prism with a ~10 mm thickness. Scale bar: 1 cm. All data are expressed as mean ± standard deviation. Significance is indicated as ***($p < 0.001$).
Abbreviations: GelMA: Gelatin methacryloyl; IL: Ionic liquid.

3 and seeded onto GelMA/IL hydrogels with laponite concentrations ranging from 0% to 1%. The Alamar Blue assay was used to evaluate the proliferation of the differentiated neurons, and there was a significant increase in cell proliferation from Day 1 to Day 3 across all groups (Figure 5G).

4. Discussion

Extrusion 3D printing of GelMA without a rheological additive is possible[10,12,16]; however, achieving consistent shape fidelity is dependent on printing conditions and GelMA concentration. The primary challenge lies in fabricating an injectable and extrudable soft hydrogel (Young's modulus < 10 kPa) suitable for nerve tissue engineering applications. Our research indicates that incorporating laponite into 5% GelMA/20% IL does not compromise the hydrogel's inherent softness but significantly enhances its rheological properties and printability.

The shear-thinning properties, critical for extrusion-based printing, were significantly improved with the addition of laponite, as evidenced by the increasing flow behavior index. This enhancement makes the hydrogel well-suited for extrusion-based 3D printing, indicated by an n index of less than 0.33.[45] Additionally, the increasing flow consistency index signifies a rise in the initial viscosity of the hydrogel at low shear rates, which is essential for maintaining shape fidelity post-printing. Shape recoverability, evaluated through 3TT, was assessed by measuring viscosity recovery at high and low shear rates. All groups exhibited similar viscosity stability at high shear rates. However, the addition of laponite significantly increased viscosity stability at low shear rates, indicating faster recovery and better maintenance of shape fidelity after printing. Structures that were 3D-printed with GelMA/IL/laponite retained better structural integrity post-printing, exhibiting a lower normalized line width compared to the GelMA/IL hydrogel. This finding, correlated with the increased stability at low shear rate and flow consistency index, further validates the suitability of GelMA/IL/laponite as a hydrogel for extrusion 3D printing.

The porosity of hydrogels plays a crucial role in modulating interactions between cells and tissues and facilitating cellular penetration into the scaffold during both 2D culture and 3D cell encapsulation.[46,47] Our study found that adding laponite does not alter the porous nature of the GelMA-based hydrogel. The large pore size remains suitable for cell penetration and growth, essential for effective tissue engineering.[47–49]

Previous studies have demonstrated that there is no significant difference in the Young's modulus of the hydrogel until the laponite concentration reaches 2% or more.[45] Our study corroborates these findings, showing that the addition of laponite did not compromise the hydrogel's inherent softness. While previous studies only examined the printability aspects of laponite addition to GelMA, our study used laponite as a drug release system in a conductive hydrogel for nerve tissue engineering. Furthermore, it has been proven that hydrogel stiffness below 10 kPa is beneficial for neuronal and astrocyte differentiation, aligning with the Young's modulus of many human soft tissues, which ranges from 1 to 10 kPa.[42–44]

In vitro degradation tests are reliable indicators of *in vivo* performance under physiological conditions. Controllable degradation is beneficial for long-term tissue regeneration and sustained drug release.[50,51] The addition of laponite attenuated the degradation rate, likely due to the electrostatic force between the nanoclay particles, which consolidates the polymer network of the hydrogel over time.

Previously, we investigated the effect of different IL concentrations on 5% GelMA hydrogel, identifying 5% GelMA/20% IL as the most conductive formulation while retaining softness, flexibility, and biocompatibility. In this study, we further explored the impact of laponite on the hydrogel's conductivity. Our results show that laponite does not affect the hydrogel's conductivity, likely because the laponite nanoclay already forms clusters that do not hinder the motion of free ions in the hydrogel. Moreover, the ionic conductivity of the optimized hydrogel was measured at approximately 30 mS/cm. This value is highly relevant for neural interface applications, as it matches and slightly exceeds the native tissues, including nerves, with an electrical conductivity that ranges up to 6 mS/cm.[52] By matching the native electrical microenvironment, the hydrogel minimizes impedance mismatch at the tissue–scaffold interface, which is critical for effective signal integration.

Laponite's high drug adsorption capacity is primarily attributed to laponite–drug ionic interactions, which can vary depending on the charge distribution within the nanoplates.[53,54] Owing to the anisotropic surface charges of laponite, positively charged drugs tend to be more easily adsorbed onto the negatively charged surface of the nanoplates. Additionally, the size of the drugs can affect their adsorption based on the matrix's porosity. Laponite nanoparticles can spatially localize drugs on the surface of the charged nanodiscs, a method extensively studied for *in situ* delivery of chemotherapeutics, wound healing, and nerve regeneration.[17,55–60] Recent studies have confirmed the efficacy of GDNF-loaded hydrogels in nerve regeneration.[61,62] However, these hydrogels are often

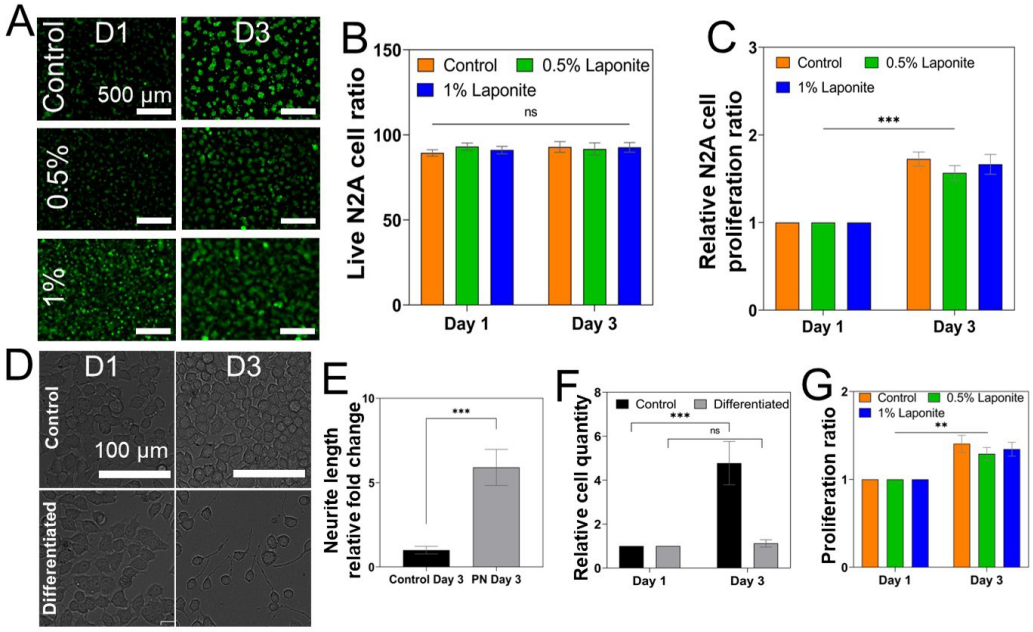

Figure 5. Biological characterization of hydrogels. (A) Live staining of two-dimensional seeded N2A cells on 5% GelMA/20% IL/0–1% on laponite, Days 1 and 3. (B) Quantification of live N2A cell ratio on Days 1 and 3. (C) Relative N2A cell proliferation ratio on 5% GelMA/20% IL/0–1% laponite from Day 1 to Day 3. (D) Brightfield images of the control (undifferentiated) and differentiated N2A cells on Day 3. Scale bar: 100 μm;. (E) Neurite length analysis and (F) relative cell density calculation of the undifferentiated and differentiated N2A cells. (G) Relative neuron proliferation ratio on 5% GelMA/20% IL/0–1% laponite from Day 1 to Day 3. All data are expressed as mean ± standard deviation. Significance is indicated as **($p < 0.01$), **($p < 0.001$) and ns (not significant).
Abbreviations: GelMA: Gelatin methacryloyl; IL: Ionic liquid.

limited by rapid *in vivo* degradation, which restricts their long-term effectiveness.[63,64]

Alternative approaches, such as fabricating GDNF-loaded microspheres and seeding them into GelMA-based hydrogels, have been explored to prolong sustained release up to 32 days.[65] However, fabrication of polymeric-based microspheres and encapsulation of growth factors into microspheres are not trivial and expensive.[66] Furthermore, this method faces challenges, including high initial burst rates, low encapsulation efficiency, migration away from the injection site, incomplete release, and instability of the encapsulated proteins.[67–71] By simply blending laponite with a biocompatible hydrogel, Wang *et al.*[57] fabricated a laponite/heparin hydrogel loaded with fibroblast growth factor 4, which has been shown to achieve a sustained release of fibroblast growth factor 4 over 35 days and enhance spinal cord injury recovery *in vivo*.

The mechanism of GDNF in nerve repair is well-established.[72,73] GDNF is upregulated by Schwann cells of the distal sciatic motor nerve stump immediately after peripheral nerve injury, but decreases after long-term denervation.[74,75] GDNF acts as a mitogen and attractant for Schwann cells and also reduces neuronal apoptosis.[76,77] Schwann cells, recruited by GDNF, aid neurite outgrowth by physically and chemically guiding the growth cone toward its target motor unit. Retinoic acid, a metabolite of vitamin A, is a common inducer of cell differentiation and can induce various types of cells to differentiate into neurons.[78–81]

In this study, both GDNF and retinoic acid were utilized. These molecules are positively charged, which strengthens their interaction with laponite.[82–84] Positively charged proteins, such as ribonuclease A and lysozyme, tend to form larger and more stable complexes with laponite, resulting in a slower release profile compared to negatively charged proteins like bovine serum albumin.[85] Laponite can effectively reduce the initial burst release of both proteins and extracellular vesicles, allowing for tunable release times.[86,87] GDNF drug release test was analyzed up to 168 h (seven days) as the doubling time for most cell types is between 24 and 72 h.[88] The retinoic acid drug release test was performed only up to 72 h (three days), as N2A cells differentiate into neurons in less than two days.[78,89] In our study, both GDNF and retinoic acid achieved a slower release rate with 1% laponite compared to the control group. This demonstrates laponite's potential to attract positively charged molecules and maintain steady and prolonged electrostatic interactions during

drug release.

Enhancing cell attachment to the matrix is critically important for cell survival. Without appropriate attachment, cells may undergo anoikis, a form of programmed cell death.[90] GelMA hydrogels closely resemble some essential properties of the ECM due to the presence of cell-attaching and matrix metalloproteinase-responsive peptide motifs, which allow cells to attach, proliferate, and spread within GelMA-based scaffolds.[91] Neuro-2a, also known as N2A, are mouse neuroblastoma cells. They are neuron precursors and can be differentiated into neurons.[89] In this study, N2A cells continued to proliferate from Day 1 to Day 3 across all groups. The addition of laponite did not affect the ECM-mimicking nature of GelMA, with all groups achieving a live cell ratio higher than 90% on Day 3.

Neuronal damage or degeneration is a hallmark of neurological diseases. Regulating neurogenesis and neuronal differentiation is vital for developing therapies that promote neuronal regeneration or synaptic network reconstruction.[92] N2A cells possess the ability to differentiate into both immature and mature neurons, which enhances neuronal regeneration and synaptic network reconstruction, thereby promoting nerve regeneration in tissue engineering applications.[79,92] Cell proliferation and differentiation exhibited a notable inverse relationship.[93] After switching to differentiation medium, N2A cell proliferation decreased, resulting in lower cell density compared to the control group. Neurite outgrowth began on Day 1, with elongation and branching essential for developing functional networks and promoting nerve regeneration.

Neurite extension and branching are key cellular activities for creating functional networks and facilitating nerve regeneration.[94–97] Differentiated neurons were harvested on Day 3 and transferred to GelMA/IL/laponite hydrogel for continued growth over three additional days. Alamar Blue assay results indicated a positive trend in neuron growth across all groups, confirming that the GelMA/IL/laponite hydrogel supports neuron growth and maturation effectively. Altogether, these results indicate that the GelMA/IL/laponite hydrogel offers a multifunctional platform with enhanced printability, sustained drug delivery, and biocompatibility, making it a strong candidate for biofabricated scaffolds in neural tissue engineering and related applications.

5. Conclusion

In conclusion, the incorporation of laponite into GelMA/IL hydrogels significantly enhanced their rheological properties without compromising softness or porosity, making them highly suitable for *in situ* extrusion-based 3D printing. Crucially, by limiting the laponite content to 1% *w*/*v*, we successfully engineered a construct that mimics the softness of native neural tissue to support neuronal differentiation, while simultaneously ensuring the structural fidelity required for high-resolution 3D printing. Laponite-modified hydrogels improved shear-thinning behavior while supporting cell viability and proliferation. Additionally, these hydrogels enabled sustained release of retinoic acid and GDNF, essential for neuron differentiation and nerve regeneration. These findings indicate that laponite-enhanced GelMA/IL hydrogels address current limitations in 3D printing for nerve tissue engineering by providing matched electromechanical properties and improved shape fidelity. This advancement paves the way for developing more effective hydrogel-based drug delivery systems and biomimetic scaffolds for regenerative medicine and nerve tissue engineering applications.

Acknowledgments

This research was partially carried out using the Core Technology Platforms resources at New York University Abu Dhabi. The graphical abstract and Figure 1A were created in BioRender. Elkhoury, K. (2025) https://BioRender.com/66sn81h and https://BioRender.com/2u9y1d1, respectively. We acknowledge Dr. Gopinathan Janarthanan for helping with the extrusion 3D printing of the construct presented in Figure 4F,G.

Funding

SV acknowledges the Early Career Research Grant (RB907) from the NYU Discovery Fund for Human Health for supporting this work.

Conflict of interest

Sanjairaj Vijayavenkataraman serves as the Editorial Board Member of the journal, but was not in any way involved in the editorial and peer-review process conducted for this paper, directly or indirectly. Other authors declare they have no competing interests.

Author contributions

Conceptualization: Jiarui Zhou, Sanjairaj Vijayavenkataraman
Data Curation: Jiarui Zhou, Kamil Elkhoury, Abhay Menon
Formal analysis: Jiarui Zhou, Kamil Elkhoury
Investigation: Jiarui Zhou, Kamil Elkhoury, Abhay Menon
Methodology: Jiarui Zhou, Kamil Elkhoury, Sanjairaj Vijayavenkataraman
Visualization: Jiarui Zhou, Kamil Elkhoury
Validation: Jiarui Zhou, Kamil Elkhoury
Resources: Sanjairaj Vijayavenkataraman

Supervision: Sanjairaj Vijayavenkataraman
Writing – original draft: Jiarui Zhou, Kamil Elkhoury
Writing – review & editing: Sanjairaj Vijayavenkataraman

Ethics approval and consent to participate

Not applicable.

Consent for publication

Not applicable.

Availability of data

All data is available in the manuscript.

References

1. Vijayavenkataraman S, Yan W-C, Lu WF, Wang C-H, Fuh JYH. 3D bioprinting of tissues and organs for regenerative medicine. *Adv Drug Deliv Rev.* 2018;132:296-332.

   doi: 10.1016/j.addr.2018.07.004

2. Mani MP, Sadia M, Jaganathan SK, *et al.* A review on 3D printing in tissue engineering applications. *J Polym Eng.* 2022;42(3):243-265.

   doi: 10.1515/polyeng-2021-0059

3. Saini G, Segaran N, Mayer J, Saini A, Albadawi H, Oklu R. Applications of 3D Bioprinting in Tissue Engineering and Regenerative Medicine. *J Clin Med.* 2021;10(21):4966.

   doi: 10.3390/jcm10214966

4. Acierno D, Patti A. Fused Deposition Modelling (FDM) of Thermoplastic-Based Filaments: Process and Rheological Properties—An Overview. *Materials*. 2023;16(24):7664.

   doi: 10.3390/ma16247664

5. Ferretti P, Santi GM, Leon-Cardenas C, Fusari E, Cristofori M, Liverani A. Production readiness assessment of low cost, multi-material, polymeric 3D printed moulds. *Heliyon*. 2022;8(10):e11136.

   doi: 10.1016/j.heliyon.2022.e11136

6. Sood AK, Ohdar RK, Mahapatra SS. Experimental investigation and empirical modelling of FDM process for compressive strength improvement. *J Adv Res.* 2012;3(1):81-90.

   doi: 10.1016/j.jare.2011.05.001

7. Li J, Wu C, Chu PK, Gelinsky M. 3D printing of hydrogels: Rational design strategies and emerging biomedical applications. *Mater Sci Eng R Rep.* 2020;140:100543.

   doi: 10.1016/j.mser.2020.100543

8. Herrada-Manchón H, Fernández MA, Aguilar E. Essential Guide to Hydrogel Rheology in Extrusion 3D Printing: How to Measure It and Why It Matters? *Gels*. 2023;9(7):517.

   doi: 10.3390/gels9070517

9. He Y, Yang F, Zhao H, Gao Q, Xia B, Fu J. Research on the printability of hydrogels in 3D bioprinting. *Sci Rep*. 2016;6(1)doi:10.1038/srep29977

10. Leu Alexa R, Iovu H, Ghitman J, *et al.* 3D-Printed Gelatin Methacryloyl-Based Scaffolds with Potential Application in Tissue Engineering. *Polymers*. 2021;13(5):727.

    doi: 10.3390/polym13050727

11. Aldana AA, Valente F, Dilley R, Doyle B. Development of 3D bioprinted GelMA-alginate hydrogels with tunable mechanical properties. *Bioprinting*. 2021;21:e00105.

    doi: 10.1016/j.bprint.2020.e00105

12. Ding H, Illsley NP, Chang RC. 3D Bioprinted GelMA Based Models for the Study of Trophoblast Cell Invasion. *Sci Rep*. 2019;9(1).

    doi: 10.1038/s41598-019-55052-7

13. Grosskopf AK, Saouaf OA, Lopez Hernandez H, Appel EA. Gelation and yielding behavior of polymer–nanoparticle hydrogels. *J Polym Sci.* 2021;59(22):2854-2866.

    doi: 10.1002/pol.20210652

14. Xu P, Shang Z, Yao M, Li X. Mechanistic insight into improving strength and stability of hydrogels via nano-silica. *J Mol Liq.* 2022;357:119094.

    doi: 10.1016/j.molliq.2022.119094

15. Yoon J, Han H, Jang J. Nanomaterials-incorporated hydrogels for 3D bioprinting technology. *Nano Converg.* 2023/11/15 2023;10(1)

    doi: 10.1186/s40580-023-00402-5

16. Dong L, Bu Z, Xiong Y, *et al.* Facile extrusion 3D printing of gelatine methacrylate/Laponite nanocomposite hydrogel with high concentration nanoclay for bone tissue regeneration. *Int J Biol Macromol.* 2021;188:72-81.

    doi: 10.1016/j.ijbiomac.2021.07.199

17. Dawson JI, Kanczler JM, Yang XB, Attard GS, Oreffo ROC. Clay Gels For the Delivery of Regenerative Microenvironments. *Adv Mater.* 2011/06/10 2011;23(29):3304-3308.

    doi: 10.1002/adma.201100968

18. Dawson JI, Oreffo ROC. Clay: New Opportunities for Tissue Regeneration and Biomaterial Design. *Adv Mater*. 2013;25(30):4069-4086.

    doi: 10.1002/adma.201301034

19. Cidonio G, Glinka M, Kim Y-H, *et al.* Nanoclay-based 3D printed scaffolds promote vascular ingrowth ex vivo and generate bone mineral tissue in vitro and in vivo. *Biofabrication*. 2020/05/11 2020;12(3):035010.

    doi: 10.1088/1758-5090/ab8753

20. Cidonio G, Alcala-Orozco CR, Lim KS, *et al.* Osteogenic and angiogenic tissue formation in high fidelity nanocomposite Laponite-gelatin bioinks. *Biofabrication*. 2019;11(3):035027.

doi: 10.1088/1758-5090/ab19fd

21. Tan Y, Xu S, Wu R, Du J, Sang J, Wang J. A gradient Laponite-crosslinked nanocomposite hydrogel with anisotropic stress and thermo-response. *Appl Clay Sci.* 2017;148:77-82.

    doi: 10.1016/j.clay.2017.08.004

22. Sheikhi A, Afewerki S, Oklu R, Gaharwar AK, Khademhosseini A. Effect of ionic strength on shear-thinning nanoclay–polymer composite hydrogels. *Biomater Sci*. 2018;6(8):2073-2083.

    doi: 10.1039/c8bm00469b

23. Ruzicka B, Zaccarelli E. A fresh look at the Laponite phase diagram. *Soft Matter*. 2011;7(4):1268.

    doi: 10.1039/c0sm00590h

24. Ng WL, Yeow CHE, Huang X, Lee S, Yeong WY. Physically cross-linked gelatin bio-inks with enhanced printability, degradation and mechanical robustness for multi-modal bioprinting. *Interdiscip Med.* 2025;3(4):e20250058.

    doi: 10.1002/INMD.20250058

25. Gunduz O, Ustundag CB, Sengor M, editors. *Biomaterials for Neural Tissue Engineering*. Elsevier; 2023.

26. Elkwood AI, Holland NR, Arbes SM, *et al.* Nerve allograft transplantation for functional restoration of the upper extremity: case series. *J Spinal Cord Med.* 2011;34(2):241-247.

    doi: 10.1179/107902611x12972448729521

27. Singh VK, Haq A, Tiwari M, Saxena AK. Approach to management of nerve gaps in peripheral nerve injuries. *Injury*. 2022;53(4):1308-1318.

    doi: 10.1016/j.injury.2022.01.031

28. Supra R, K Agrawal D. Peripheral Nerve Regeneration: Opportunities and Challenges. *J Spine Res Surg.* 2023;05(01).

    doi: 10.26502/fjsrs0052

29. Zhou J, Vijayavenkataraman S. 3D-printable conductive materials for tissue engineering and biomedical applications. *Bioprinting*. 2021;24:e00166.

    doi: 10.1016/j.bprint.2021.e00166

30. Carvalho CR, Chang W, Silva-Correia J, Reis RL, Oliveira JM, Kohn J. Engineering Silk Fibroin-Based Nerve Conduit with Neurotrophic Factors for Proximal Protection after Peripheral Nerve Injury. *Adv Healthc Mater.* 2020;10(2).

    doi: 10.1002/adhm.202000753

31. Nectow AR, Marra KG, Kaplan DL. Biomaterials for the Development of Peripheral Nerve Guidance Conduits. *Tissue Eng Part B Rev.* 2012;18(1):40-50.

    doi: 10.1089/ten.teb.2011.0240

32. Zhao Y, Liang Y, Ding S, Zhang K, Mao HQ, Yang Y. Application of conductive PPy/SF composite scaffold and electrical stimulation for neural tissue engineering. *Biomaterials*. 2020;255:120164.

    doi: 10.1016/j.biomaterials.2020.120164

33. Fukaya Y, Iizuka Y, Sekikawa K, Ohno H. Bio ionic liquids: room temperature ionic liquids composed wholly of biomaterials. *Green Chem.* 2007;9(11):1155.

    doi: 10.1039/b706571j

34. Kuchenbuch A, Giernoth R. Ionic Liquids Beyond Simple Solvents: Glimpses at the State of the Art in Organic Chemistry. *ChemistryOpen*. 2015;4(6):677-681.

    doi: 10.1002/open.201500113

35. Lei Z, Chen B, Koo YM, MacFarlane DR. Introduction: Ionic Liquids. *Chem Rev*. 2017;117(10):6633-6635.

    doi: 10.1021/acs.chemrev.7b00246

36. Kuchenbuch A, Giernoth R. Ionic Liquids Beyond Simple Solvents: Glimpses at the State of the Art in Organic Chemistry. *ChemistryOpen*. 2015;4(6):677-681.

    doi: 10.1002/open.201500113

37. Gomes JM, Silva SS, Reis RL. Biocompatible ionic liquids: fundamental behaviours and applications. *Chem Soc Rev*. 2019;48(15):4317-4335.

    doi: 10.1039/c9cs00016j

38. Noshadi I, Walker BW, Portillo-Lara R, *et al.* Engineering Biodegradable and Biocompatible Bio-ionic Liquid Conjugated Hydrogels with Tunable Conductivity and Mechanical Properties. *Sci Rep*. 2017;7(1):4345.

    doi: 10.1038/s41598-017-04280-w

39. Krishnadoss V, Kanjilal B, Masoumi A, *et al.* Programmable bio-ionic liquid functionalized hydrogels for in situ 3D bioprinting of electronics at the tissue interface. *Mater Today Adv.* 2023;17:100352.

    doi: 10.1016/j.mtadv.2023.100352

40. Zhou J, Elkhoury K, Saghar Soman S, Vijayavenkataraman S. Biofabrication of tri-layered nerve guide conduits for peripheral nerve regeneration: Synergizing melt-electrowriting of polymeric fibers and extrusion-based 3D bioprinting. *Int J Bioprinting.* 2025.

    doi: 10.36922/ijb025040032

41. Menon A, Elkhoury K, Zahraa A, *et al.* Digital light processing 3D printing of dual cross-linked meniscal scaffolds with enhanced physical and biological properties. *Adv Compos Hybrid Mater.* 2024;8(1).

    doi: 10.1007/s42114-024-01196-8

42. Saha K, Keung AJ, Irwin EF, *et al.* Substrate Modulus Directs Neural Stem Cell Behavior. *Biophys J*. 2008;95(9):4426-4438.

    doi: 10.1529/biophysj.108.132217

43. Seidlits SK, Khaing ZZ, Petersen RR, *et al.* The effects

of hyaluronic acid hydrogels with tunable mechanical properties on neural progenitor cell differentiation. *Biomaterials*. 2010;31(14):3930-3940.

doi: 10.1016/j.biomaterials.2010.01.125

44. Liu J, Zheng H, Poh P, Machens H-G, Schilling A. Hydrogels for Engineering of Perfusable Vascular Networks. *Int J Mol Sci*. 2015/07/14 2015;16(7):15997-16016.

doi: 10.3390/ijms160715997

45. Davern JW, Hipwood L, Bray LJ, Meinert C, Klein TJ. Addition of Laponite to gelatin methacryloyl bioinks improves the rheological properties and printability to create mechanically tailorable cell culture matrices. *APL Bioeng*. 2024/01/08 2024;8(1).

doi: 10.1063/5.0166206

46. Ma Y, Wang X, Su T, Lu F, Chang Q, Gao J. Recent Advances in Macroporous Hydrogels for Cell Behavior and Tissue Engineering. *Gels*. 2022/09/21 2022;8(10):606.

doi: 10.3390/gels8100606

47. Annabi N, Nichol JW, Zhong X, *et al.* Controlling the Porosity and Microarchitecture of Hydrogels for Tissue Engineering. *Tissue Eng Part B Rev.* 2010;16(4):371-383.

doi: 10.1089/ten.teb.2009.0639

48. Zeltinger J, Sherwood JK, Graham DA, Müeller R, Griffith LG. Effect of Pore Size and Void Fraction on Cellular Adhesion, Proliferation, and Matrix Deposition. *Tissue Eng.* 2001;7(5):557-572.

doi: 10.1089/107632701753213183

49. Žigon-Branc S, Markovic M, Van Hoorick J, *et al.* Impact of Hydrogel Stiffness on Differentiation of Human Adipose-Derived Stem Cell Microspheroids. *Tissue Eng Part A*. 2019;25(19-20):1369-1380.

doi: 10.1089/ten.tea.2018.0237

50. Holloway JL, Ma H, Rai R, Burdick JA. Modulating hydrogel cross-link density and degradation to control bone morphogenetic protein delivery and in vivo bone formation. *J. Control Release.* 2014;191:63-70.

doi: 10.1016/j.jconrel.2014.05.053

51. Rambhia KJ, Ma PX. Controlled drug release for tissue engineering. *J Control Release*. 2015;219:119-128.

doi: 10.1016/j.jconrel.2015.08.049

52. Li YM, Ji Y, Meng YX, *et al.* Neural Tissue-Like, not Supraphysiological, Electrical Conductivity Stimulates Neuronal Lineage Specification through Calcium Signaling and Epigenetic Modification. *Adv Sci*. 2024;11(35):e2400586.

doi: 10.1002/advs.202400586

53. Chakraborty J, Majumder N, Sharma A, Prasad S, Ghosh S. 3D bioprinted silk-reinforced Alginate-Gellan Gum constructs for cartilage regeneration. *Bioprinting*. 2022;28:e00232.

doi: 10.1016/j.bprint.2022.e00232

54. Munoz-Perez E, Perez-Valle A, Igartua M, Santos-Vizcaino E, Hernandez RM. High resolution and fidelity 3D printing of Laponite and alginate ink hydrogels for tunable biomedical applications. *Biomater Adv*. 2023;149:213414.

doi: 10.1016/j.bioadv.2023.213414

55. Ghadiri M, Chrzanowski W, Rohanizadeh R. Antibiotic eluting clay mineral (Laponite®) for wound healing application: an in vitro study. *J Mater Sci Mater Med.* 2014;25(11):2513-2526.

doi: 10.1007/s10856-014-5272-7

56. Kiaee G, Mostafalu P, Samandari M, Sonkusale S. A pH-Mediated Electronic Wound Dressing for Controlled Drug Delivery. *Adv Healthc Mater.* 2018;7(18).

doi: 10.1002/adhm.201800396

57. Wang C, Gong Z, Huang X, *et al.* An injectable heparin-Laponite hydrogel bridge FGF4 for spinal cord injury by stabilizing microtubule and improving mitochondrial function. *Theranostics*. 2019;9(23):7016-7032.

doi: 10.7150/thno.37601

58. Wang G, Maciel D, Wu Y, *et al.* Amphiphilic Polymer-Mediated Formation of Laponite-Based Nanohybrids with Robust Stability and pH Sensitivity for Anticancer Drug Delivery. *ACS Appl Mater Interfaces.* 2014;6(19):16687-16695.

doi: 10.1021/am5032874

59. Zhang M, Bai Y, Xu C, *et al.* Novel optimized drug delivery systems for enhancing spinal cord injury repair in rats. *Drug Deliv.* 2021;28(1):2548-2561.

doi: 10.1080/10717544.2021.2009937

60. Zhou B, Wu B, Wang J, *et al.* Drug-mediation formation of nanohybrids for sequential therapeutic delivery in cancer cells. *Colloids Surf. B Biointerfaces.* 2018;163:284-290.

doi: 10.1016/j.colsurfb.2017.12.046

61. Cai Y, Chen Y, Zhang G, *et al.* The GDNF-gel/HA-Mg conduit promotes the repair of peripheral nerve defects by regulating PPAR-γ/RhoA/ROCK signaling pathway. *iScience*. 2024;27(2):108969.

doi: 10.1016/j.isci.2024.108969

62. Qiu S, Rao Z, He F, *et al.* Decellularized nerve matrix hydrogel and glial-derived neurotrophic factor modifications assisted nerve repair with decellularized nerve matrix scaffolds. *J Tissue Eng Regen Med.* 2020;14(7):931-943.

doi: 10.1002/term.3050

63. Hosseinzadeh B, Ahmadi M. Degradable hydrogels: Design mechanisms and versatile applications. *Mater Today Sustain*. 2023;23:100468.

doi: 10.1016/j.mtsust.2023.100468

64. Patel G, Dalwadi C. Recent Patents on Stimuli Responsive Hydrogel Drug Delivery System. *Recent Pat Drug Deliv Formul.* 2013;7(3):206-215.

doi: 10.2174/18722113076661311181416 00

65. Xing MMQ, Zhuang H, Bu S, Hua L, Darabi MA, Cao X. Gelatin-methacrylamide gel loaded with microspheres to deliver GDNF in bilayer collagen conduit promoting sciatic nerve growth. *Int J Nanomed.* 2016:1383.

doi: 10.2147/ijn.s96324

66. Fadia NB, Bliley JM, DiBernardo GA, *et al.* Long-gap peripheral nerve repair through sustained release of a neurotrophic factor in nonhuman primates. *Sci Transl Med.* 2020;12(527)eaav7753.

doi: 10.1126/scitranslmed.aav7753

67. Ansary RH, Awang MB, Rahman MM. Biodegradable Poly(D,L-lactic-co-glycolic acid)-Based Micro/ Nanoparticles for Sustained Release of Protein Drugs - A Review. *Trop J Pharm Res.* 2014;13(7):1179.

doi: 10.4314/tjpr.v13i7.24

68. Blanco D, Alonso MaJ. Protein encapsulation and release from poly(lactide-co-glycolide) microspheres: effect of the protein and polymer properties and of the co-encapsulation of surfactants. *Eur J Pharm Biopharm.* 1998;45(3):285-294.

doi: 10.1016/s0939-6411(98)00011-3

69. Estey T, Kang J, Schwendeman SP, Carpenter JF. BSA Degradation Under Acidic Conditions: A Model For Protein Instability During Release From PLGA Delivery Systems. *J Pharm Sci.* 2006;95(7):1626-1639.

doi: 10.1002/jps.20625

70. Gavali KV, Kengar MD, Chavan KV, Anekar VP, Khan NI. A Review on Microsphere and it's Application. *Asian J Pharm Res.* 2019;9(2):123.

doi: 10.5958/2231-5691.2019.00020.0

71. Kang J, Schwendeman SP. Comparison of the effects of Mg(OH)2 and sucrose on the stability of bovine serum albumin encapsulated in injectable poly(d,l-lactide-co-glycolide) implants. *Biomaterials.* 2002;23(1):239-245.

doi: 10.1016/s0142-9612(01)00101-6

72. Lin L-FH, Doherty DH, Lile JD, Bektesh S, Collins F. GDNF: a Glial Cell Line-Derived Neurotrophic Factor for Midbrain Dopaminergic Neurons. *Science.* 1993;260(5111):1130-1132.

doi: 10.1126/science.8493557

73. Zhang L, Ma Z, Smith GM, *et al.* GDNF-enhanced axonal regeneration and myelination following spinal cord injury is mediated by primary effects on neurons. *Glia.* 2009;57(11):1178-1191.

doi: 10.1002/glia.20840

74. Xu P, Rosen KM, Hedstrom K, *et al.* Nerve injury induces glial cell line-derived neurotrophic factor (gdnf) expression in schwann cells through purinergic signaling and the pkc-pkd pathway. *Glia.* 2013;61(7):1029-1040.

doi: 10.1002/glia.22491

75. Höke A, Gordon T, Zochodne DW, Sulaiman OAR. A decline in glial cell-line-derived neurotrophic factor expression is associated with impaired regeneration after long-term Schwann cell denervation. Article. *Exp Neurol.* 2002;173(1):77-85.

doi: 10.1006/exnr.2001.7826

76. Airaksinen MS, Saarma M. The GDNF family: Signalling, biological functions and therapeutic value. *Nat Rev Neurosci.* 2002;3(5):383-394.

doi: 10.1038/nrn812

77. Yue P, Gao L, Wang X, Ding X, Teng J. Intranasal Administration of GDNF Protects Against Neural Apoptosis in a Rat Model of Parkinson's Disease Through PI3K/Akt/GSK3β Pathway. *Neurochem Res.* 2017;42(5):1366-1374.

doi: 10.1007/s11064-017-2184-1

78. Kumar M, Katyal A. Data on retinoic acid and reduced serum concentration induced differentiation of Neuro-2a neuroblastoma cells. *Data Brief.* 2018;21:2435-2440.

doi: 10.1016/j.dib.2018.11.097

79. Namsi A, Nury T, Hamdouni H, *et al.* Induction of Neuronal Differentiation of Murine N2a Cells by Two Polyphenols Present in the Mediterranean Diet Mimicking Neurotrophins Activities: Resveratrol and Apigenin. *Diseases.* 2018;6(3):67.

doi: 10.3390/diseases6030067

80. Shimizu S, Kondo M, Miyamoto Y, Hayashi M. Foxa(HNF3) Upregulates Vitronectin Expression during Retinoic Acid-induced Differentiation in Mouse Neuroblastoma Neuro2a Cells. *Cell Struct Funct.* 2002;27(4):181-188.

doi: 10.1247/csf.27.181

81. Du Y-J, Dong S-Z, You Q, Gong Q, Han Y-Q, Pi R. Role of miR-124 in the regulation of retinoic acid-induced Neuro-2A cell differentiation. *Neural Regen Res.* 2020;15(6):1133.

doi: 10.4103/1673-5374.270417

82. Runeberg-Roos P, Penn RD. Improving therapeutic potential of GDNF family ligands. *Cell Tissue Res.* 2020;382(1):173-183.

doi: 10.1007/s00441-020-03256-z

83. Esteves M, Cristóvão AC, Saraiva T, *et al.* Retinoic acid-loaded polymeric nanoparticles induce neuroprotection in a mouse model for Parkinson's disease. *Front Aging Neurosci.* 2015;7.

doi: 10.3389/fnagi.2015.00020

84. Ye T, Pollack GH. Do aqueous solutions contain net charge? *PLOS ONE*. 2022/10/27 2022;17(10):e0275953.

doi: 10.1371/journal.pone.0275953

85. Rodrigo MJ, Cardiel MJ, Fraile JM, Mayoral JA, Pablo LE, Garcia-Martin E. Laponite for biomedical applications: An ophthalmological perspective. *Materials Today Bio*. 2024;24:100935.

doi: 10.1016/j.mtbio.2023.100935

86. Hu H, Dong L, Bu Z, *et al.* miR-23a-3p-abundant small extracellular vesicles released from Gelma/nanoclay hydrogel for cartilage regeneration. *J Extracell Vesicles*. 2020;9(1).

doi: 10.1080/20013078.2020.1778883

87. Man K, Barroso IA, Brunet MY, *et al.* Controlled Release of Epigenetically-Enhanced Extracellular Vesicles from a GelMA/Nanoclay Composite Hydrogel to Promote Bone Repair. *Int J Mol Sci*. 2022;23(2):832.

doi: 10.3390/ijms23020832

88. Korzynska A, Zychowicz M. A Method of Estimation of the Cell Doubling Time on Basis of the Cell Culture Monitoring Data. *Biocybern Biomed Engineering*. 2008;28:75-82.

89. Martín D, Ruano D, Yúfera A, Daza P. Electrical pulse stimulation parameters modulate N2a neuronal differentiation. *Cell Death Discov.* 2024;10(1).

doi: 10.1038/s41420-024-01820-y

90. Rago AP, Napolitano AP, Dean DM, Chai PR, Morgan JR. Miniaturization of an Anoikis assay using non-adhesive micromolded hydrogels. *Cytotechnology*. 2007;56(2):81-90.

doi: 10.1007/s10616-007-9116-x

91. Yue K, Trujillo-de Santiago G, Alvarez MM, Tamayol A, Annabi N, Khademhosseini A. Synthesis, properties, and biomedical applications of gelatin methacryloyl (GelMA) hydrogels. *Biomaterials*. 2015;73:254-271.

doi: 10.1016/j.biomaterials.2015.08.045

92. An J, Chen B, Tian D, Guo Y, Yan Y, Yang H. Regulation of Neurogenesis and Neuronal Differentiation by Natural Compounds. *Curr Stem Cell Res Ther*. 2022;17(8):756-771.

doi: 10.2174/1574888X16666210907141447

93. Ruijtenberg S, van den Heuvel S. Coordinating cell proliferation and differentiation: Antagonism between cell cycle regulators and cell type-specific gene expression. *Cell Cycle*. 2016;15(2):196-212.

doi: 10.1080/15384101.2015.1120925

94. Nasser TIN, Spencer GE. Neurite Outgrowth. In: *Reference Module in Biomedical Sciences*. Amsterdam, The Netherlands: Elsevier; 2017.

95. Meldolesi J. Neurite outgrowth: This process, first discovered by Santiago Ramon y Cajal, is sustained by the exocytosis of two distinct types of vesicles. *Brain Res Rev.* 2011;66(1-2):246-255.

doi: 10.1016/j.brainresrev.2010.06.004

96. Paganoni S, Ferreira A. Neurite extension in central neurons: a novel role for the receptor tyrosine kinases Ror1 and Ror2. *J Cell Sci*. 2005;118(2):433-446.

doi: 10.1242/jcs.01622

97. Valtorta F, Leoni C. Molecular mechanisms of neurite extension. *Philos Trans R. Soc Lond Ser B Biol. Sci*. 1999;354(1381):387-394.

doi: 10.1098/rstb.1999.0391